Mohui Jin[1]
College of Engineering,
South China Agricultural University,
Guangzhou 510642, China
e-mail: jinmohui@163.com

Xianmin Zhang
School of Mechanical and
Automotive Engineering,
South China University of Technology,
Guangzhou 510641, China

Zhou Yang
College of Engineering,
South China Agricultural University,
Guangzhou 510642, China

Benliang Zhu
School of Mechanical and
Automotive Engineering,
South China University of Technology,
Guangzhou 510641, China

Jacobian-Based Topology Optimization Method Using an Improved Stiffness Evaluation

A Jacobian-based topology optimization method is recently proposed for compliant parallel mechanisms (CPMs), in which the CPMs' Jacobian matrix and characteristic stiffness are optimized simultaneously to achieve kinematic and stiffness requirement, respectively. Lately, it is found that the characteristic stiffness fails to ensure a valid topology result in some particular cases. To solve this problem, an improved stiffness evaluation based on the definition of stiffness is adopted in this paper. This new stiffness evaluation is verified and compared with the characteristic stiffness by using several design examples. In addition, several typical benchmark problems (e.g., displacement inverter, amplifier, and redirector) are solved by using the Jacobian-based topology optimization method to show its general applicability. [DOI: 10.1115/1.4038332]

1 Introduction

Compliant mechanisms are elastic structures that can transmit force or motion from input to output. Due to the combined characteristics of mechanism and structure, the analysis and design of compliant mechanisms are more challenging than that of rigid-body mechanisms. There are two main synthesis approaches for compliant mechanisms, i.e., rigid-body replacement approach [1–3] and topology optimization approach [4–7].

The rigid-body replacement approach has a wide design scope including all kinds of degree-of-freedom (DOF) compliant mechanisms. This approach synthesizes most of compliant parallel mechanisms (CPMs), whose synthesis method is the focus of this paper, by replacing the kinematic joints of existing rigid-body mechanisms with flexure hinges. Thus, the compliant mechanisms designed by this approach rely on the topologies of rigid-body mechanisms. While this approach is successful in designing multi-DOF CPMs for precision applications, it is limited by the fact that a compliant mechanism may still be unable to fully reproduce the motion of its rigid-body counterpart even using rigorous analysis and optimization techniques [8]. Moreover, this approach cannot select the best topology for a specific problem currently, which is quite important for developing mechanisms with high performance.

The topology optimization approach regards the synthesis of compliant mechanism as finding out the optimal material distribution within a given design domain, by maximizing the motion or force transmission between specific input and output ports. Due to this advantage, the topology optimization approach has been successfully applied to the synthesis problems of multiple input and output ports [5,9–13], multiple materials or physics [9–11], three-dimensional simple compliant mechanisms [14–16], etc. The compliant mechanisms designed by this approach possess structural type of topology, i.e., no flexure hinges, which is different from the flexure hinge-based mechanisms obtained by the rigid-body replacement approach.

To introduce the idea of topology optimization into the design scope of the rigid-body replacement approach, our previous works [17–19] tried to synthesize the flexure-based compliant mechanisms with simple motion based on the idea of topology optimization. Lum et al. [20–22] presented a hybrid topological and structural optimization method. This method first synthesizes the compliant joints with the optimal stiffness characteristics by topology optimization. The resulting compliant joints are then assembled into a CPM based on existing rigid-body mechanism topology.

Recently, we proposed a Jacobian-based topology optimization method [23] for the optimal synthesis of planar CPMs. Traditional topology optimization methods realize multiple outputs by predefining specific output displacements at output ports. The premise of this realization is that the position and direction of output ports are known. However, the output motion of multi-DOF CPMs is unknown. The traditional way of predefining specific output ports cannot be applied to multi-DOF CPMs topology optimization directly. To solve this problem, Jacobian matrix [24,25] is introduced into the field of topology optimization by the proposed method. The Jacobian matrix describes all the freedoms of CPM's mobile platform in a unified and concise form, and contains the information of CPM's DOF and direct kinematics simultaneously. By optimizing the Jacobian matrix, one can synthesize a compliant mechanism with desired DOF (mechanism's function) and optimized direct kinematics (mechanism's performance). In addition to the above kinematic realization, the mechanism's input and output characteristic stiffness [26,27] (C-stiffness for short) are also optimized to achieve enough stiffness to bear the external loads.

Lately, we found that the C-stiffness fails to ensure a valid topology result in some particular problems. In this paper, an improved stiffness evaluation based on its definition is incorporated into the problem formulation, and will be compared with the C-stiffness formulation by using several design problems.

The rest of this paper is organized as follows: Section 2 describes the problem formulations of Jacobian-based topology optimization method. Section 3 illustrates the topology analysis of CPMs. The sensitivity analysis and optimization algorithm are described in Sec. 4. Section 5 gives numerical examples to verify the stiffness formulation. The conclusions are presented in Sec. 6.

2 Jacobian-Based Topology Optimization Method

2.1 Problem Description. The topology of a CPM is determined by the number, arrangement, and topology structures of its

[1]Corresponding author.

Contributed by the Design Automation Committee of ASME for publication in the Journal of Mechanical Design. Manuscript received February 25, 2017; final manuscript received September 28, 2017; published online November 9, 2017. Assoc. Editor: James K. Guest.

constituent compliant limbs. The proposed method regards the problem of CPMs topology optimization as finding the best topology of compliant limbs within several given design domains.

A CPM composed of n compliant limbs is shown in Fig. 1. The mechanism's compliant limbs are assumed to be synthesized within n predefined design domains, $\Gamma = \{\Omega_1, \Omega_2, \ldots, \Omega_n\}$. The corresponding design variables to these design domains are illustrated by $\mathbf{X} = \{\mathbf{X}_1, \mathbf{X}_2, \ldots, \mathbf{X}_n\}$. The number of compliant limbs, n, is determined by the number of CPM's DOF. The position of input points a_i $(i = 1, 2, \ldots, n)$ and output point o is defined by designers.

2.2 Properties of Jacobian Matrix. The kinematics of multi-DOF CPMs is much more complicated than that of the compliant mechanisms designed by current topology optimization methods. Since the motion of CPMs is unknown, i.e., the output trajectory of the mobile platform is not fixed, we cannot use fixed output loads to define its output motion any more. Considering the application situation, the Jacobian matrix, which is previously used in analysis of rigid-body mechanisms and flexure-based CPMs, is introduced into topology optimization as an alternative kinematic formulation. As shown in Eq. (1), the Jacobian matrix $\mathbf{J}$ describes transmission relation between the displacements of input and output freedoms, i.e., forward kinematics of the CPM

$$\mathbf{U}_o = \mathbf{J}\mathbf{U}_a \tag{1}$$

where $\mathbf{U}_o = [u_x, u_y, \theta_z]^{\mathrm{T}}$ contains the three freedoms' displacement of output point o at the mobile platform, and $\mathbf{U}_a = [u_1, u_2, \ldots, u_n]^{\mathrm{T}}$ is the vector of input displacements at input points a_i. Since the compliant mechanisms are usually driven by linear motion actuators, we limit the displacements in $\mathbf{U}_a$ to the translational freedoms of input points.

The element J_{ji} in $\mathbf{J}$ represents the geometry advantage (GA) between the jth freedom of $\mathbf{U}_o$ and the ith input. If all the elements of the jth row in $\mathbf{J}$ are equal or close to zero, all the inputs in $\mathbf{U}_a$ will not produce displacement in the jth freedom of mobile platform, i.e., this freedom is suppressed. While the other freedoms corresponding to nonzero row vectors are considered as the CPM's DOF. By maximizing the absolute value of the elements in the nonzero row vectors, the forward kinematics and motion transmission performance of CPM can be optimized. Thus, the Jacobian matrix contains the information of CPM's function and performance simultaneously. By optimizing the Jacobian matrix, we can synthesize a compliant mechanism with desired DOF to realize the mechanism's function and optimized direct kinematics to achieve higher performance.

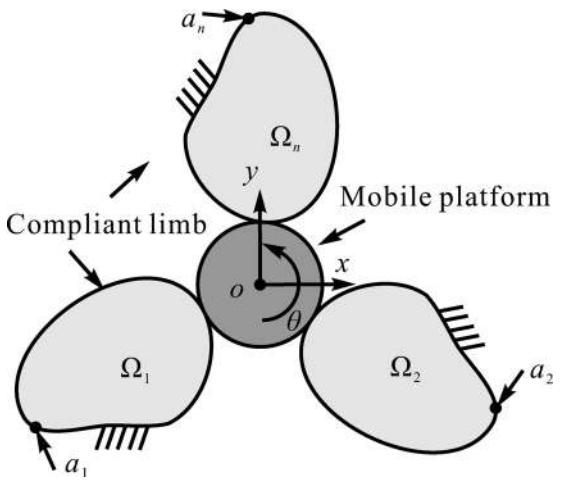

Fig. 1 General design domain for planar CPMs

2.3 Problem Formulation. The objective function of CPMs topology optimization used in Ref. [23] is developed on the basis of Chen and Wang's formulation [26,27] that utilizes the C-stiffness. This paper tries to modify the formulation using a new stiffness evaluation that calculates the stiffness based on its definition.

2.3.1 Differences Between C-Stiffness and Stiffness. The formulation proposed by Chen and Wang is used for the compliant mechanisms with single input and single output. Take the compliant system shown in Fig. 2 as an example to illustrate the formulation. For this compliant system, the relationship between forces (f_{in} and f_{out}) and displacements (u_{in} and u_{out}) at input and output ports can be described by a mechanism stiffness matrix $\mathbf{K}_m$ [28] shown in the following equation:

$$\begin{bmatrix} f_{\mathrm{in}} \\ f_{\mathrm{out}} \end{bmatrix} = \underbrace{\begin{bmatrix} k_{11} & k_{12} \\ k_{21} & k_{22} \end{bmatrix}}_{\mathbf{K}_m} \begin{bmatrix} u_{\mathrm{in}} \\ u_{\mathrm{out}} \end{bmatrix} \tag{2}$$

The diagonal elements of the mechanism stiffness matrix $\mathbf{K}_m$ [28] are the C-stiffness [26]. As shown in Eq. (3), they incorporate the C-stiffness at input and output ports (k_{11} and k_{22}) into the formulation to achieve topology optimization of hinge-free compliant mechanisms

$$\min - \underbrace{e^{-(\mathrm{GA}-\mathrm{GA}^*)^2}}_{f} \underbrace{k_{11}k_{22}}_{S} \tag{3}$$

where GA is the geometry advantage of the mechanism, and GA* is the desired geometry advantage, f and S represent the kinematic and stiffness requirement, respectively.

According to Eq. (2), the physical meanings of k_{11} and k_{21} are the forces that should be acted on input and output ports, if $u_{\mathrm{in}} = 1$ and $u_{\mathrm{out}} = 0$ are expected. The input C-stiffness k_{11} just describes part of the stiffness relationship between f_{in} and u_{in}, and so does the output C-stiffness k_{22}.

On the contrary, the stiffness based on its definition can fully describe the force and displacement relationship at one specific freedom. To obtain the input and output stiffness of this simple compliant system, the input and output compliance are first calculated according to the physical meaning of compliance. Let $f_{\mathrm{in}} = 1$ and $f_{\mathrm{out}} = 0$, and solve Eq. (2). The resulting input displacement u_{in} is the input compliance

$$u_{\mathrm{in}} = \frac{k_{22}}{k_{11}k_{22} - k_{12}k_{21}} \tag{4}$$

Let $f_{\mathrm{in}} = 0$ and $f_{\mathrm{out}} = 1$, and solve Eq. (2). The resulting output displacement u_{out} is the output compliance

$$u_{\mathrm{out}} = \frac{k_{11}}{k_{11}k_{22} - k_{12}k_{21}} \tag{5}$$

The inverse of input and output compliance are the input and output stiffness, respectively

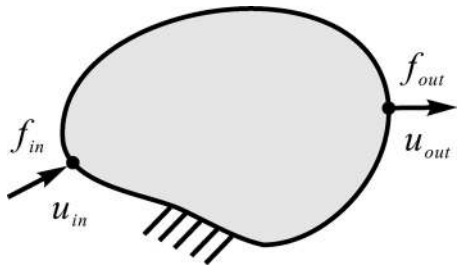

Fig. 2 A compliant system with single input and single output

$$k_{\text{in}} = u_{\text{in}}^{-1} = k_{11} - k_{12}k_{21}/k_{22}$$
$$k_{\text{out}} = u_{\text{out}}^{-1} = k_{22} - k_{12}k_{21}/k_{11} \tag{6}$$

By comparing k_{11} and k_{22} with k_{in} and k_{out}, respectively, C-stiffness is part of the stiffness. While the C-stiffness has successfully evaluated the mechanism's stiffness property in many design problems, some problems show that the stiffness is more reliable than C-stiffness. Thus, this paper will modify the formulations of Jacobian-based topology optimization method by replacing the C-stiffness with stiffness.

2.3.2 Formulations Using New Stiffness Evaluation. As can be seen in Eq. (3), the kinematic requirement f and stiffness requirement S are two conflicting subobjectives. On one hand, the mechanism should be soft enough to deform and deliver motion. On the other hand, it should be stiff enough to transmit forces to the mobile platform and bear the external force. A general problem formulation for CPMs topology optimization can be written as follows:

$$\begin{aligned} \min \quad & \zeta(\mathbf{X}) = -f^{\omega} S^{(1-\omega)} \\ s.t. \quad & V(\mathbf{X}) \le V_o \end{aligned} \tag{7}$$

where ω $(0 < \omega < 1)$ is the weight indicating the relative significance of kinematic requirement f. $V(\mathbf{X})$ is the volume fraction of topology candidate, and V_o is the allowed volume fraction.

The kinematic requirement f has two different forms according to the design problem. The first form of kinematic requirement f_1 is suitable for the CPMs whose kinematics is simple enough to be predefined by designers. This form is to force the Jacobian matrix $\mathbf{J}$ of CPM to be close to a desired Jacobian matrix $\mathbf{J}^*$ by minimizing the differences between J_{ji} and J_{ji}^*, which are the elements of $\mathbf{J}$ and $\mathbf{J}^*$, respectively. As a result, the desired DOF and kinematic properties of CPM can be expressed in the desired Jacobian matrix $\mathbf{J}^*$

$$\begin{aligned} &\max\ f_1 = e^{-\sum (J_{ji} - J_{ji}^*)^2} \\ &j = 1, 2, \ldots, 3 \quad i = 1, 2, \ldots, n \end{aligned} \tag{8}$$

The second form of kinematic requirement f_2 is suitable for the CPMs with complex kinematics. This form tries to maximize the motion in desired freedoms J_j^d and suppress the rest J_j^c

$$\max f_2 = e^{-\sum J_j^c} \prod J_j^d \tag{9}$$

where J_j evaluates the workspace in the jth freedom, which is the quadratic sum of the elements in corresponding row vector shown in Eq. (10). J_j^d is the workspace of a desired freedom, while J_j^c is the workspace of a constrained freedom. The natural exponential function forces each J_j^c to be close to zero

$$J_j = \sum_{i=1}^{n} J_{ji}^2 \tag{10}$$

In our previous work [23], the stiffness requirement S is achieved by maximizing the input and output C-stiffness of the CPM. This paper uses the stiffness calculated by its definition as a new stiffness evaluation instead of the C-stiffness. Mathematically, the stiffness requirement is formulated as the product of the input stiffness k_{in}^i and output stiffness k_{out}^i

$$\max S = \prod_{i=1}^{n} k_{\text{in}}^i k_{\text{out}}^i \tag{11}$$

The calculation of Jacobian matrix $\mathbf{J}$, input and output stiffness will be illustrated in Secs. 3.3 and 3.4, respectively.

2.4 Unification of the Units in Rotational and Translational Freedoms. Since the units in rotational and translational freedoms are different, it is unfair to compare the parameters in rotational and translational freedoms directly during the optimization. Thus, the characteristic length [29,30] l_c is introduced in this paper. Based on the characteristic length l_c, we can define equivalent moment $\tilde{M}$ and equivalent rotational displacement $\tilde{\theta}_z$ as follows:

$$\begin{aligned} \tilde{M} &= M/l_c \\ \tilde{\theta}_z &= \theta_z l_c \end{aligned} \tag{12}$$

For the Jacobian matrix, each element J_{ji} is the ratio of the jth freedom of $\mathbf{U}_o$ and the ith input. Since all the inputs are translational freedoms, only the rotational displacement θ_z in $\mathbf{U}_o$ should be transformed into equivalent rotation displacement $\tilde{\theta}_z$. Thus, the elements in the third row vector of $\mathbf{J}$ are multiplied by l_c to obtain equivalent Jacobian matrix $\tilde{\mathbf{J}}$

$$\tilde{J}_{3i} = J_{3i} l_c, \quad i = 1, 2, \ldots, n \tag{13}$$

For the input and output stiffness, the output stiffness related to rotational freedom should be transformed into equivalent rotational stiffness. The relationship among the applied moment M, rotational stiffness k_θ, and rotational displacement θ_z is as follows:

$$M = k_\theta \theta_z \tag{14}$$

Solve the moment M and rotational displacement θ_z in Eq. (12), and substitute them into Eq. (14)

$$\tilde{M} l_c = k_\theta \tilde{\theta}_z / l_c \tag{15}$$

The equivalent rotational stiffness $\tilde{k}_\theta$ is calculated as follows:

$$\tilde{k}_\theta = \tilde{M}/\tilde{\theta}_z = k_\theta / l_c^2 \tag{16}$$

3 Topology Analysis

This section shows how the Jacobian matrix, and input and output stiffnesses of CPMs can be obtained by using the finite element analysis and matrix methods [31].

3.1 Discretization and Parameterization. One advantage of using multiple design domains is that the compliant limbs of CPM can be discretized, parameterized, and analyzed separately in their local coordinates. A compliant limb in its local coordinate is shown in Fig. 3, and consists of design domain Ω_i and part of the mobile platform Ω_p^i. The compliant limb $(\Omega_i + \Omega_p^i)$ is discretized by using the quadrilateral elements that possess three freedoms (u_x, u_y, θ_z) at each node, and parameterized by the simplified isotropic material with penalization scheme [32]. The stiffness matrix of the ith compliant limb can be obtained by the following equation:

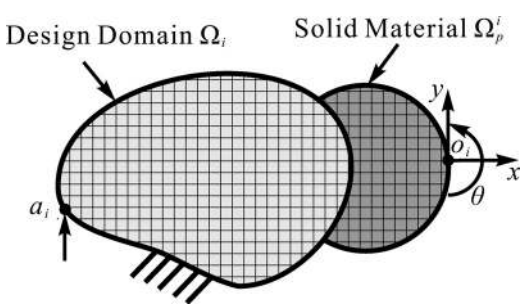

Fig. 3 Stiffness modeling schematic for the *i*th compliant limb

$$\mathbf{K}_i(\mathbf{X}_i) = \sum_{e=1}^{N_i} (x^e)^\rho \mathbf{K}_e + \sum_{e=1}^{N_p^i} \mathbf{K}_e$$
$$0 < x_{\min}^e \le x^e \le 1, \quad x^e \in \mathbf{X}_i \tag{17}$$

where N_i is the number of the elements in design domain Ω_i, N_p^i is the number of the elements in Ω_p^i, $\mathbf{K}_e$ is the element stiffness matrix in the global level, x^e is the material density (design variable) of each element in Ω_i with value between the lower limit $x_{\min}^e$ (void) and 1 (solid), ρ is the penalty factor, the elements in Ω_p^i are solid.

3.2 Stiffness Modeling of CPMs. For a compliant limb in its local coordinate (as shown in Fig. 3), only the input freedom at point a_i and the three freedoms of endpoint o_i are considered in its stiffness modeling. First, a compliance matrix $\mathbf{C}_{ao}^i$ that characterizes the compliance relationship between these four concerned freedoms is calculated according to physical meaning of compliance. Four load cases $\mathbf{F}_j$ $(j = 1, 2, \ldots, 4)$, in which a unit dummy load is applied to each concerned freedom of a_i and o_i in sequence, are used to calculate corresponding displacements by solving the following equation:

$$\mathbf{F}_j = \mathbf{K}_i \mathbf{U}_j, \quad j = 1, 2, \ldots, 4 \tag{18}$$

The physical meaning of element C_{jk} in a compliance matrix $\mathbf{C}$ is the displacement of the jth freedom due to a unit load that only acts on the kth freedom. According to this physical meaning, the element of $\mathbf{C}_{ao}^i$ is obtained by Eq. (19). The displacements of the four concerned freedoms in displacement vector $\mathbf{U}_k$ form the kth column in $\mathbf{C}_{ao}^i$

$$\mathbf{C}_{ao}^i(j,k) = \mathbf{F}_j^{\mathrm{T}} \mathbf{U}_k, \quad j,k = 1, 2, \ldots, 4 \tag{19}$$

Then, the compliance of endpoint o_i is transferred into the coordinate of the output point o by a transformation matrix $\mathbf{T}_i^o$, whereas the compliance of the input freedom at a_i remains in its local coordinate. The inverse of the resulting compliance matrix, i.e., stiffness matrix $\mathbf{K}_{ao}^i$, is shown in Eq. (20). For more information about the transformation matrix $\mathbf{T}_i^o$, please refer to Refs. [31,33].

$$\mathbf{K}_{ao}^i = \left(\begin{bmatrix} 1 & \mathbf{0} \\ \mathbf{0} & \mathbf{T}_i^o \end{bmatrix} \otimes \mathbf{C}_{ao}^i \right)^{-1} \tag{20}$$

where 1 is to keep the compliance of the input freedom at a_i remain in its local coordinate, and the notation $\otimes$ is defined as follows:

$$\mathbf{A} \otimes \mathbf{C} = \mathbf{A}\mathbf{C}\mathbf{A}^{\mathrm{T}} \tag{21}$$

Finally, the stiffness model of compliant limbs will be combined into the stiffness model of CPM. The stiffness related to the output point o in $\mathbf{K}_{ao}^i$ of all the compliant limbs are superimposed to form stiffness of the output point o at mobile platform, while the stiffness of all the input freedoms at points a_i $(i = 1, 2, \ldots, n)$ remain in their local coordinates. The transformation is shown in Eq. (22). The resulting $\mathbf{K}_m$ is the mechanism stiffness matrix that characterizes the stiffness relationship between the n input freedoms and the three freedoms of output point o

$$\mathbf{K}_m = \begin{bmatrix} 1 & \mathbf{0} & \mathbf{0} & \mathbf{0} & \cdots & \mathbf{0} & \mathbf{0} \\ \mathbf{0} & \mathbf{0} & 1 & \mathbf{0} & \cdots & \mathbf{0} & \mathbf{0} \\ \vdots & \vdots & \vdots & \vdots & \ddots & \vdots & \vdots \\ \mathbf{0} & \mathbf{0} & \mathbf{0} & \mathbf{0} & \cdots & 1 & \mathbf{0} \\ \mathbf{0} & \mathbf{I} & \mathbf{0} & \mathbf{I} & \cdots & \mathbf{0} & \mathbf{I} \end{bmatrix} \otimes \begin{bmatrix} \mathbf{K}_{ao}^1 & \mathbf{0} & \cdots & \mathbf{0} & \mathbf{0} \\ \mathbf{0} & \mathbf{K}_{ao}^2 & \cdots & \mathbf{0} & \mathbf{0} \\ \vdots & \vdots & \ddots & \vdots & \vdots \\ \mathbf{0} & \mathbf{0} & \cdots & \mathbf{K}_{ao}^{n-1} & \mathbf{0} \\ \mathbf{0} & \mathbf{0} & \cdots & \mathbf{0} & \mathbf{K}_{ao}^n \end{bmatrix} \tag{22}$$

3.3 Kinematic Analysis of CPMs. According to the input and output freedoms of the CPM, the mechanism's displacements are partitioned into two sets $\mathbf{U}_a$ and $\mathbf{U}_o$, respectively, for displacements of the input and output freedoms. As shown in Eq. (23), the mechanism loads are also partitioned into two sets as $\mathbf{F}_a$ and $\mathbf{F}_o$, accordingly. This would in effect partition the mechanism stiffness matrix $\mathbf{K}_m$ into the following form:

$$\begin{bmatrix} \mathbf{F}_a \\ \mathbf{F}_o \end{bmatrix} = \underbrace{\begin{bmatrix} \mathbf{K}_{11} & \mathbf{K}_{12} \\ \mathbf{K}_{21} & \mathbf{K}_{22} \end{bmatrix}}_{\mathbf{K}_m} \begin{bmatrix} \mathbf{U}_a \\ \mathbf{U}_o \end{bmatrix} \tag{23}$$

Assuming that there is no external load applied to the mobile platform of CPMs, i.e., $\mathbf{F}_o = \mathbf{0}$, by solving the second equation in Eq. (23), the relationship between the input displacement $\mathbf{U}_a$ and output displacement $\mathbf{U}_o$, i.e., the Jacobian matrix $\mathbf{J}$, can be obtained

$$\mathbf{J} = -\mathbf{K}_{22}^{-1} \mathbf{K}_{21} \tag{24}$$

3.4 Input and Output Stiffness of CPMs. By using the mechanism stiffness matrix $\mathbf{K}_m$, we can calculate the input and output stiffness of CPMs according to the physical meaning of compliance. As shown in Eq. (25), $n+3$ unit load vectors ($\mathbf{F}_{\text{in}}^i$ and $\mathbf{F}_{\text{out}}^j$) are applied to the freedoms of $\mathbf{K}_m$ in sequence to obtain corresponding displacement vectors $\mathbf{U}_{\text{in}}^i$ and $\mathbf{U}_{\text{out}}^j$

$$\begin{aligned} \mathbf{F}_{\text{in}}^i &= \mathbf{K}_m \mathbf{U}_{\text{in}}^i, \quad i = 1, 2, \ldots, n \\ \mathbf{F}_{\text{out}}^j &= \mathbf{K}_m \mathbf{U}_{\text{out}}^j, \quad j = 1, 2, 3 \end{aligned} \tag{25}$$

The displacement of the freedom where the unit load is applied is the compliance in this freedom, which can be extracted from the corresponding displacement vector by using the related unit load vector. The inverse of these compliances are the stiffness in the input and output freedoms of this CPM

$$\begin{aligned} k_{\text{in}}^i &= ((\mathbf{F}_{\text{in}}^i)^{\mathrm{T}} \mathbf{U}_{\text{in}}^i)^{-1}, \quad i = 1, 2, \ldots, n \\ k_{\text{out}}^j &= ((\mathbf{F}_{\text{out}}^j)^{\mathrm{T}} \mathbf{U}_{\text{out}}^j)^{-1}, \quad j = 1, 2, 3 \end{aligned} \tag{26}$$

4 Sensitivity Analysis

The sensitivity of the objective function discussed in Sec. 2.3.2 is determined by the sensitivities of J_{ji}, k_{in}^i, and k_{out}^j. The sensitivity of J_{ji} can be extracted from sensitivity of $\mathbf{J}$, which is calculated as follows:

$$\frac{\partial \mathbf{J}}{\partial x^e} = \mathbf{K}_{22}^{-1} \frac{\partial \mathbf{K}_{22}}{\partial x^e} \mathbf{K}_{22}^{-1} \mathbf{K}_{21} - \mathbf{K}_{22}^{-1} \frac{\partial \mathbf{K}_{21}}{\partial x^e} \tag{27}$$

Since $\mathbf{K}_{22}$ and $\mathbf{K}_{21}$ are parts of $\mathbf{K}_m$, the sensitivity of $\mathbf{J}$ is determined by the sensitivity of $\mathbf{K}_m$. According to Eq. (26), the sensitivity of k_{in}^i is calculated by Eq. (28), while the sensitivity of k_{out}^j can be obtained by the same way

$$\frac{\partial k_{\text{in}}^i}{\partial x^e} = -\left(\mathbf{F}_{\text{in}}^i\right)^{\mathrm{T}} \frac{\partial \mathbf{U}_{\text{in}}^i}{\partial x^e} \left(k_{\text{in}}^i\right)^2 \tag{28}$$

where the sensitivity of $\mathbf{U}_{\text{in}}^i$ is as follows:

$$\frac{\partial \mathbf{U}_{\text{in}}^i}{\partial x^e} = -\left(\mathbf{K}_m^{-1} \frac{\partial \mathbf{K}_m}{\partial x^e} \mathbf{K}_m^{-1} \right) \mathbf{F}_{\text{in}}^i \tag{29}$$

Substitute Eq. (29) into Eq. (28), the sensitivity of k_{in}^i can be turned into the following form:

$$\frac{\partial k_{\text{in}}^i}{\partial x^e} = \left(\left(\mathbf{U}_{\text{in}}^i\right)^{\text{T}} \frac{\partial \mathbf{K}_m}{\partial x^e} \mathbf{U}_{\text{in}}^i \right) \left(k_{\text{in}}^i\right)^2 \tag{30}$$

According to Eqs. (20) and (22), the sensitivity of $\mathbf{K}_m$ is determined by the sensitivities of $\mathbf{K}_{ao}^i$

$$\frac{\partial \mathbf{K}_{ao}^i}{\partial x^e} = -\mathbf{K}_{ao}^i \left(\begin{bmatrix} 1 & \mathbf{0} \\ \mathbf{0} & \mathbf{T}_i^o \end{bmatrix} \otimes \frac{\partial \mathbf{C}_{ao}^i}{\partial x^e} \right) \mathbf{K}_{ao}^i \tag{31}$$

where the sensitivity of the element in $\mathbf{C}_{ao}^i$ can be calculated as follows:

$$\begin{aligned} \frac{\partial \mathbf{C}_{ao}^i(j,k)}{\partial x^e} &= \mathbf{F}_j^{\text{T}} \frac{\partial \mathbf{U}_k}{\partial x^e} = \mathbf{F}_j^{\text{T}} \frac{\partial}{\partial x^e} \left(\mathbf{K}_i^{-1} \mathbf{F}_k \right) \\ &= -\mathbf{F}_j^{\text{T}} \mathbf{K}_i^{-1} \frac{\partial \mathbf{K}_i}{\partial x^e} \mathbf{K}_i^{-1} \mathbf{F}_k \\ &= -\mathbf{U}_j^{\text{T}} \frac{\partial \mathbf{K}_i}{\partial x^e} \mathbf{U}_k \\ &= -\rho (x^e)^{\rho-1} \mathbf{U}_j^{\text{T}} \mathbf{K}_e \mathbf{U}_k \end{aligned} \tag{32}$$

On the basis of sensitivity analysis, the topology optimization problem is solved by modifying the 99 line MATLAB code proposed by Sigmund [34]. The optimality criteria-based optimizer and filtering technique [7] of the 99 line MATLAB code are used to update the design variables of each domain and ensure existence of solutions, respectively. For each numerical example in Sec. 5, the initial design $\mathbf{X}$ is defined by setting the material density of each element to be the value of the allowed volume fraction, i.e., $x^e = V_o$. The convergence criterion is the change in design variables, which is set to 0.005 in this paper. The move limit in the heuristic updating scheme is 0.1. The filter radius r_{min} is set to 1.2, i.e., the filter length scale d_{min} ($d_{\text{min}} = 2r_{\text{min}}$) is 2.4. It should be pointed out that the volume constraint is active during the whole optimization process. For more detail about the optimality criteria-based optimizer and filtering technique, readers can refer to Ref. [34].

5 Numerical Studies

This section will compare several topology optimization results obtained by using the C-stiffness and stiffness formulations, respectively. The artificial material properties for these examples are described as: Young's modulus is $E = 1$ GPa and Poisson's ratio is $\upsilon = 0.3$. The characteristic length l_c is set to 10 mm in this study. All the numerical examples are carried out on a computer with Intel Core *i*7 – 6700 (3.40 GHz) CPU, 8.00GB RAM, and MATLAB *R*2009*a*. Note that the filter length scale $d_{\text{min}} = 2.4$ is represented by a red bar in each figure showing the final topology.

5.1 Design of 2DOF CPMs. In this section, a 2DOF CPM will be synthesized using two asymmetrical compliant limbs within the design domain shown in Fig. 4. As can be seen, the two compliant limbs have the same size and boundary conditions. Each compliant limb is discretized by 100×100 finite elements for elastic analysis. The allowable amount of material is 20%.

5.1.1 Solved by Using f_1. Since the kinematics of 2DOF CPMs is simple enough to predefine its desired Jacobian matrix $\mathbf{J}^*$, this design problem can be solved using the first form of objective function in Eq. (8). The $\mathbf{J}^*$ for this example is given by Eq. (33), in which a_{1x} and a_{2y} are the input freedoms. The zero vector in the third row of the $\mathbf{J}^*$ means that the freedom θ_z should be suppressed, i.e., the CPM is expected to have only two translational freedoms (u_x and u_y). Moreover, the two translational freedoms are expected to be decoupled. For example, the input a_{1x} only induces the translational displacement u_x with desired geometry advantage GA* and has no impact on the other two freedoms

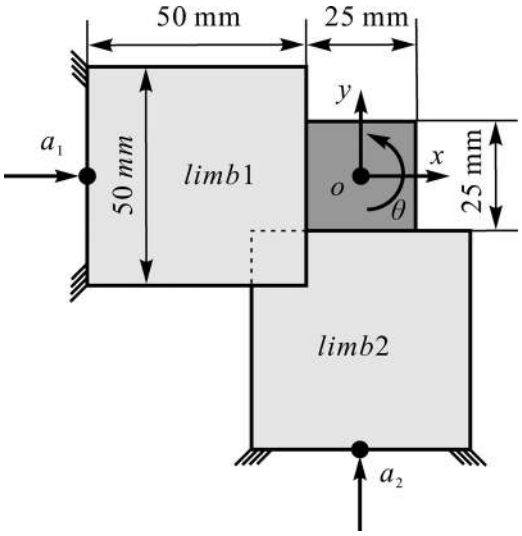

Fig. 4 Design domain for 2DOF CPMs

$$\begin{bmatrix} u_x \\ u_y \\ \theta_z \end{bmatrix} = \underbrace{\begin{bmatrix} \text{GA}^* & 0 \\ 0 & \text{GA}^* \\ 0 & 0 \end{bmatrix}}_{\mathbf{J}^*} \begin{bmatrix} a_{1x} \\ a_{2y} \end{bmatrix} \tag{33}$$

The GA* is first set to -3 and ω is set to 0.5. The corresponding topology optimization problem is solved by using the C-stiffness and stiffness formulations, respectively. The optimizations were run for 200 iterations. The resulting topologies of the two formulations are shown in Fig. 5, which shows that both of C-stiffness and stiffness formulations can obtain valid topologies in this case. Figures 6 and 7 show the iteration history of objective value, kinematic requirement f, and stiffness requirement S in the optimization process of the two formulations, respectively. It can be seen that oscillations exist in the iteration curves. The oscillations may be caused by the material distribution at some specific elements. Fortunately, the topologies at later period of iteration are stable, which can be regarded as the optimal topology. The corresponding $\mathbf{J}$ of the two final topologies are listed in the first two rows of Table 1. It should be noted that only the elements in the first column vector of $\mathbf{J}$ are displayed for brevity, since $J_{11} \simeq J_{22}$, $J_{21} \simeq J_{12}$, and $J_{31} \simeq J_{32}$. One can see that both of C-stiffness and stiffness formulations can force $\mathbf{J}$ of CPMs to be close to $\mathbf{J}^*$, i.e., the kinematics requirement f is realized. In addition, the C-stiffness (Ck_{a1} and Ck_{ox}) and stiffness (k_{a1} and k_{ox}) of the input and output ports in x-axis of the two final topologies are given in the first two rows of Table 2. The results show that both of C-stiffness and stiffness formulations realize the stiffness requirement S

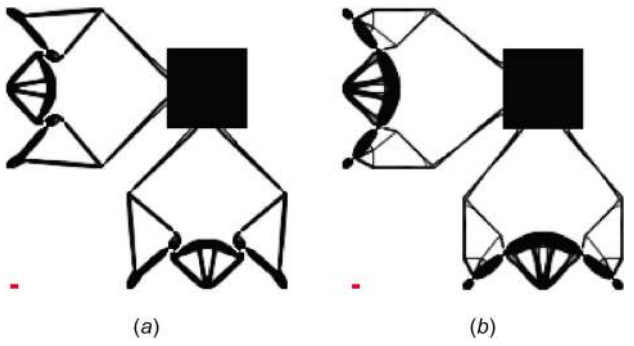

Fig. 5 Final topologies of 2DOF CPM for the case of GA* = −3 solved by (*a*) the C-stiffness ($\omega = 0.5$) and (*b*) stiffness ($\omega = 0.5$) formulations

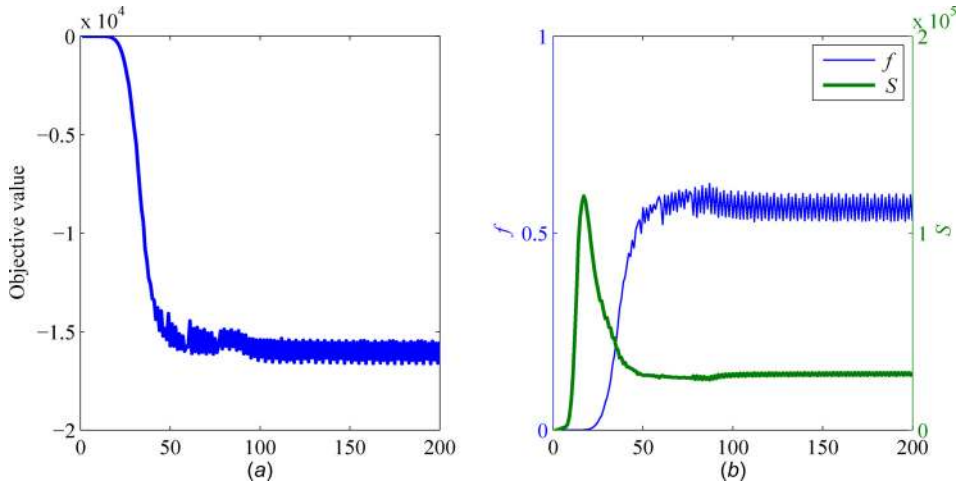

Fig. 6 Iteration history of the topology in Fig. 5(*a*): (*a*) objective value and (*b*) kinematics requirement *f* and stiffness requirement *S*

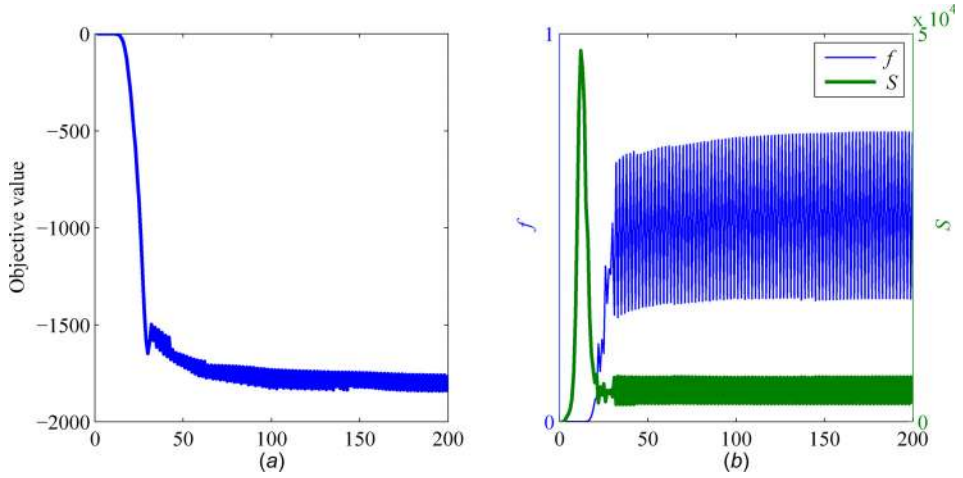

Fig. 7 Iteration history of the topology in Fig. 5(*b*): (*a*) objective value and (*b*) kinematics requirement *f* and stiffness requirement *S*

Table 1 Jacobian matrices of the final 2DOF CPMs

Formulation	GA*	J_{11}	J_{21}	J_{31}
C-stiffness	−3	−2.52	8×10^{-4}	0.02
Stiffness	−3	−2.26	1.1×10^{-3}	0.02
C-stiffness	2.5	1	0	-3.5×10^{-3}
Stiffness	2.5	2.27	-4×10^{-4}	−0.02

Table 2 Input and output stiffness of the final 2DOF CPMs

Formulation	GA*	Ck_{a1}	Ck_{ox}	k_{a1}	k_{ox}
C-stiffness	−3	38.7	4.3	11.3	1.3
Stiffness	−3	51.4	3.1	35.8	2.1
C-stiffness	2.5	101.4	101.4	2×10^{-6}	2×10^{-6}
Stiffness	2.5	77.5	6.9	42.1	3.7

effectively. The resulting output stiffness is smaller than the input stiffness to achieve GA, whereas the value of C-stiffness is larger than stiffness for the same mechanism.

However, when GA* is set to be positive, e.g., GA* = 2.5, it is found that the C-stiffness formulation fails to ensure the stiffness requirement *S* and results in invalid topologies. Figure 8(*a*) shows the final topology obtained by using the C-stiffness in the case of GA* = 2.5. Although the input and output points of the CPM are connected by solid material successfully, there is no material connection between the compliant limbs and fixed ports. Consequently, the displacements of the input and output ports in one direction are equal, i.e., $J_{11} = 1$ (in the third row of Table 1). As

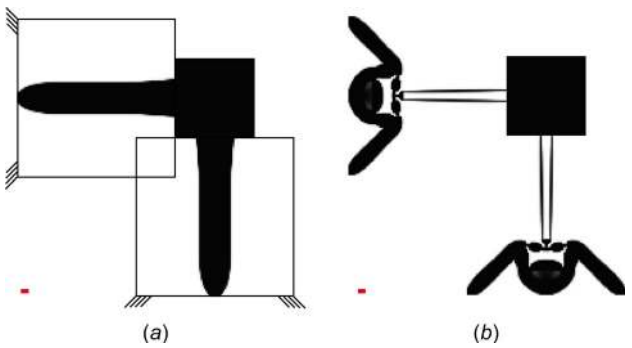

Fig. 8 Final topologies of 2DOF CPM for the case of GA* = 2.5 solved by (*a*) the C-stiffness and (*b*) stiffness ($\omega = 0.7$) formulations

shown in the third row of Table 2, the C-stiffness of the input and output ports in x-axis is 101.4 N/mm, whereas the corresponding stiffness k_{a1} and k_{ox} of this invalid topology are approximate to zero. Obviously, the C-stiffness fails to evaluate the stiffness of mechanism in this case.

Then, this problem is solved by using the stiffness formulation. The final topology is shown in Fig. 8(*b*), where ω is set to 0.7. One can see that there are valid material connections between the input, output and fixed ports of the CPM. As shown in the last rows of Tables 1 and 2, the resulting $\mathbf{J}$ is close to $\mathbf{J}^*$, e.g., $J_{11} = 2.27$. The values of its C-stiffness and stiffness are reasonable. Thus, the problem of C-stiffness is avoided and a valid final topology can be ensured by the stiffness formulation.

5.1.2 Solved by Using f_2. To compare the two forms of objective function, the 2DOF CPM design problem is also solved by using f_2 shown in Eq. (9). According to this design problem, the kinematic requirement f_2 is to maximize the workspace of the two translational freedoms and minimize the workspace of the rotational freedom, which is formulated as follows:

$$\max f_2 = e^{-J_3^c} \prod_{j=1}^{2} J_j^d \tag{34}$$

When f_2 is combined with the stiffness requirement S based on C-stiffness, the resulting final topology is similar to the topology in Fig. 8(*a*). The final topology obtained by using f_2 and stiffness based S is shown in Fig. 9. ω is set to 0.7. The corresponding Jacobian matrix is described by Eq. (35). One can see that the workspace of the two translational freedoms (u_x and u_y) is much larger than that of rotational freedom θ_z. The resulting values of J_{11} and J_{22} are positive, i.e., f_2 cannot control the sign of J_{ji} like f_1 does

$$\mathbf{J} = \begin{bmatrix} 4.19 & 0.01 \\ -0.01 & 4.20 \\ -0.01 & 0.05 \end{bmatrix} \tag{35}$$

5.2 Design of 3DOF CPMs. The second design problem of CPMs is to synthesize a 3DOF CPM with three symmetrically arranged compliant limbs. The positions of the CPM's input, output, and fixed points are shown in Fig. 10. Each design domain Ω_i is discretized by 50×80 finite elements for elastic analysis under the same boundary condition. The allowable amount of material is 20%. Since the kinematics of 3DOF CPM is complex, it is hard to predefine a desired Jacobian matrix for the optimization. The second form of kinematic requirement f_2 shown in Eq. (9) will be used in the objective function. For the planar 3DOF CPMs, no freedom should be suppressed, i.e., the design objective is to maximize the workspace of these three freedoms.

The problem is solved by using the C-stiffness and stiffness formulations, respectively. The optimization process was run for 200 iterations. Figure 11 gives the final topology of 3DOF CPM obtained by using the C-stiffness formulation and setting $\omega = 0.7$. Its corresponding Jacobian matrix $\mathbf{J}$ is shown in Eq. (36). While the final topology obtained by using the stiffness formulation ($\omega = 0.9$) and its resulting Jacobian matrix $\mathbf{J}$ is shown in Fig. 12 and Eq. (37), respectively. One can see that both of the C-stiffness and stiffness formulations are able to achieve valid topology in this example, whereas the topology obtained by the stiffness formulation is stiffer.

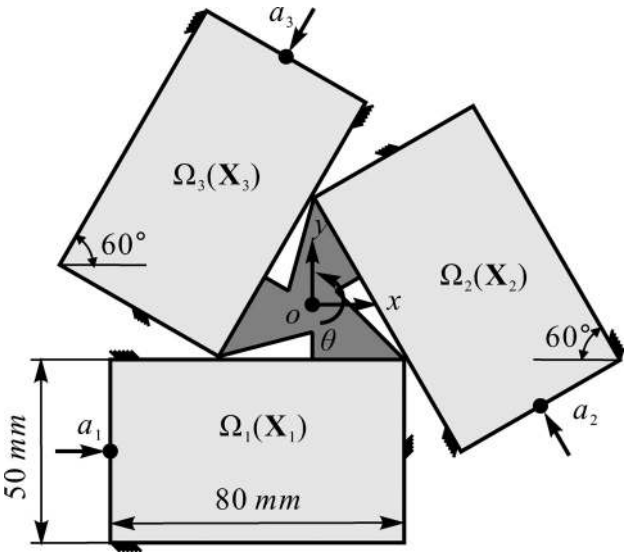

Fig. 10 Design domain for a 3DOF CPM

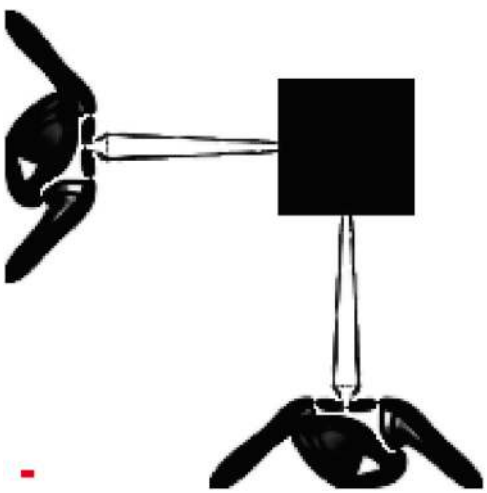

Fig. 9 Final topology of 2DOF CPM obtained by using f_2 and stiffness formulation

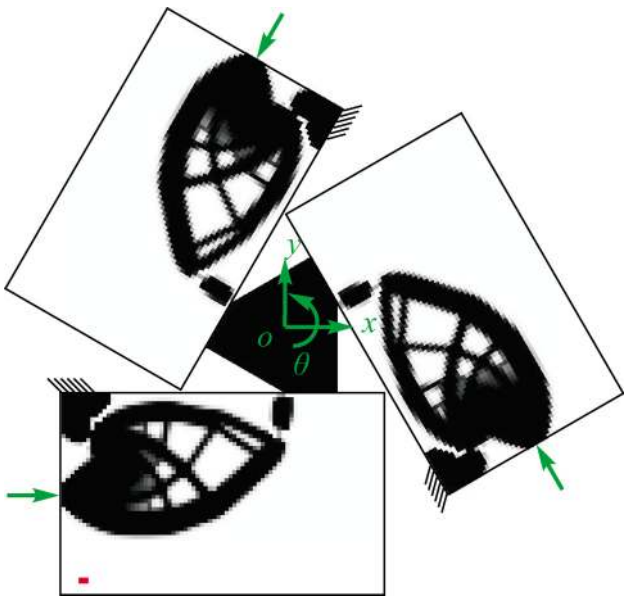

Fig. 11 Final topology of the 3DOF CPM solved by the C-stiffness formulation

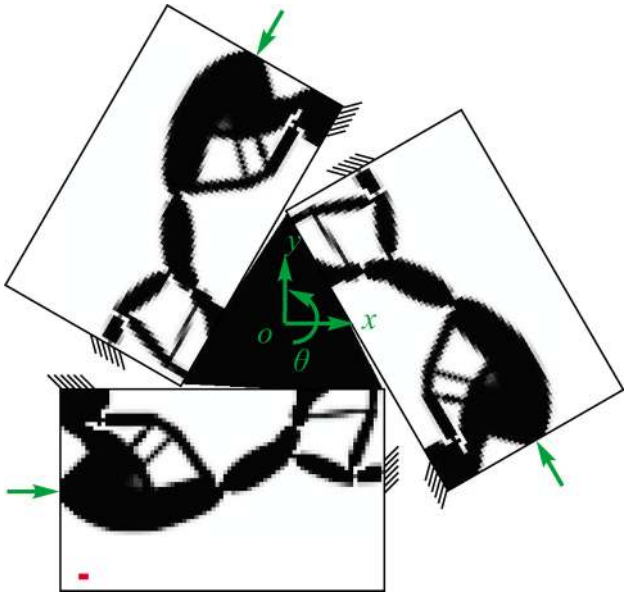

Fig. 12 Final topology of the 3DOF CPM solved by the stiffness formulation

$$\mathbf{J} = \begin{bmatrix} 0.22 & -1.79 & 1.57 \\ 1.94 & -0.78 & -1.16 \\ 0.27 & 0.27 & 0.27 \end{bmatrix} \tag{36}$$

$$\mathbf{J} = \begin{bmatrix} 0.93 & -2.18 & 1.24 \\ 1.97 & -0.18 & -1.79 \\ 0.12 & 0.12 & 0.12 \end{bmatrix} \tag{37}$$

5.3 Solving Benchmark Problems. Although the Jacobian-based topology optimization method is developed for the CPMs, this method is applicable to the typical compliant mechanisms designed by the current topology optimization methods, e.g., displacement inverter, amplifier, and redirector.

5.3.1 Displacement Inverter and Amplifier. A design problem of 1DOF compliant mechanisms using single design domain is shown in Fig. 13. The top left corner and the bottom left corner of the design domain are fixed. The input point a and output point o are in the middle of the left and right sides, respectively. The whole design domain is discretized using 100×100 finite elements for elastic analysis. The material usage is restricted to 20%. The Jacobian matrix of the 1DOF compliant mechanism is a 3×1 vector, whose desired form is shown in Eq. (38). One can see that the desired output motion of this mechanism is in the direction of x-axis, whereas the freedoms u_y and θ_z should be suppressed.

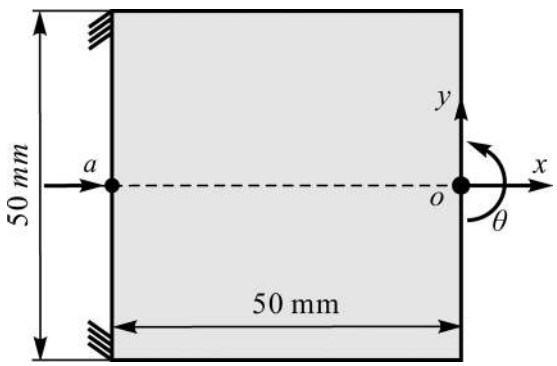

Fig. 13 Design domain for displacement inverter and amplifier

Obviously, when only the element J_{11} of Jacobian matrix is considered, our objective function is equal to the formulation proposed by Chen and Wang (Eq. (3))

$$[u_x, u_y, \theta_z]^{\mathrm{T}} = [GA^*, 0, 0]^{\mathrm{T}} a_x \tag{38}$$

When GA^* is negative, e.g., $GA^* = -3$, the design problem is to synthesize a displacement inverter. The corresponding topology optimization problem is also solved by using the C-stiffness and stiffness formulations, respectively. Figure 14(*a*) shows the resulting topology obtained by using the C-stiffness formulation and setting the weight as $\omega = 0.5$. Its corresponding Jacobian matrix is $\mathbf{J} = [-2.7, 0, 0]^{\mathrm{T}}$, i.e., the optimized GA of displacement inverter is -2.7. The C-stiffness at the input and output ports are 40.9 and 4.7 N/mm, while the stiffness at input and output ports are 6.4 and 0.7 N/mm, respectively. Figure 14(*b*) shows the resulting topology obtained by using the stiffness formulation and setting ω to 0.5. Its corresponding Jacobian matrix is $\mathbf{J} = [-2.8, 0, 0]^{\mathrm{T}}$. The C-stiffness at the input and output ports are 57.2 and 2.7 N/mm, while the stiffness at input and output ports are 41.3 and 2.0 N/mm, respectively. One can see that both of the C-stiffness and stiffness formulations can obtain valid topologies in this case.

When GA^* is positive, e.g., $GA^* = 3$, the design problem is to synthesize a displacement amplifier. It is found that the C-stiffness formulation results in the invalid topology shown in Fig. 15(*a*). Without material connected to the fixed ports, the Jacobian matrix of the resulting displacement amplifier is $\mathbf{J} = [1, 0, 0]^{\mathrm{T}}$. Both of the input and output C-stiffness are 116.1 N/mm, whereas both of the corresponding input and output stiffness are 4.3×10^{-7} N/mm. Figure 15(*b*) shows the resulting topology obtained by using the stiffness formulation and setting ω to 0.6. Its corresponding Jacobian matrix is $\mathbf{J} = [2.3, 0, 0]^{\mathrm{T}}$. The C-stiffness at the input and output ports are 79.5 and 6.2 N/mm, while the stiffness at input and output ports are 47.8 and

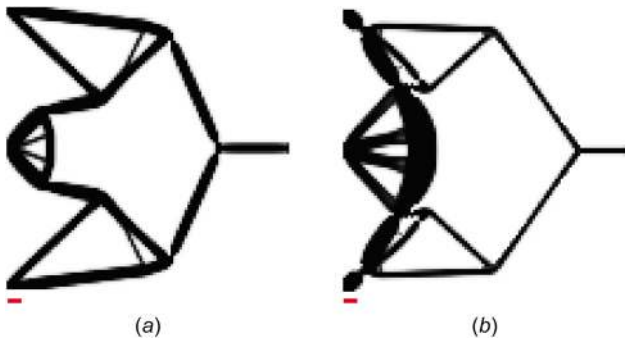

Fig. 14 Final topologies of displacement inverter for the case of $GA^* = -3$ solved by (*a*) the C-stiffness ($\omega = 0.5$) and (*b*) stiffness ($\omega = 0.5$) formulations

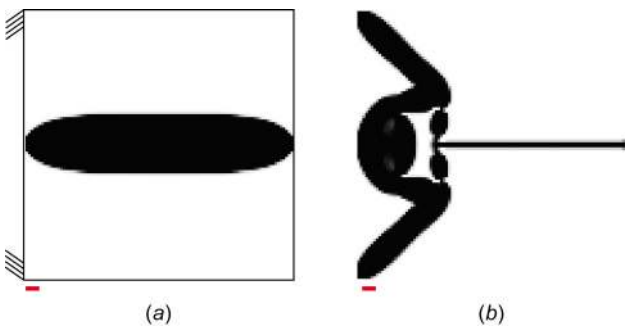

Fig. 15 Final topologies of displacement amplifier for the case of $GA^* = 3$ solved by (*a*) the C-stiffness and (*b*) stiffness ($\omega = 0.6$) formulations

3.8 N/mm, respectively. This case shows again that the C-stiffness formulation fails to ensure the stiffness requirement.

5.3.2 Solved by Using the Artificial I/O Spring and MSE/SE Formulations. There are several popular formulations developed for topology optimization of compliant mechanisms. Deepak et al. [35] have made a comparative study of these formulations. The popular artificial I/O spring and mutual strain energy/strain energy (MSE/SE) formulations are adopted here to solve the problem of displacement amplifier. In the artificial I/O spring formulation, two artificial springs are added to the input and output ports, respectively. The problem is formulated as follow:

$$\begin{aligned} &\max \quad u_{\text{out}} \\ &s.t. \quad V(\mathbf{X}) \le V_o \end{aligned} \tag{39}$$

For the problem of displacement amplifier discussed above, it is found that the artificial I/O spring formulation also results in the invalid topology shown in Fig. 15(*a*), although the stiffness values of the artificial springs have been varied from 10^{-10} to 10^{10} N/mm by ten times. On the contrary, the MSE/SE formulation (Eq. (40)) ensures the valid topology result shown in Fig. 16.

$$\begin{aligned} &\min \quad -\text{MSE} + \text{SE} \\ &s.t. \quad V(\mathbf{X}) \le V_o \end{aligned} \tag{40}$$

The computational expense of the proposed method is compared with the artificial I/O spring formulation by solving the design problem of displacement inverter in Sec. 5.3.1. It takes the artificial I/O spring formulation 47.59 s and 220 iterations to find out the solution, i.e., 216 ms per iteration. The C-stiffness formulation spends 181.5 s and 300 iterations to obtain the topology in Fig. 14(*a*), i.e., 605 ms per iteration. The stiffness formulation spends 209.37 s and 300 iterations to obtain the topology in Fig. 14(*b*), i.e., 698 ms per iteration. Obviously, the proposed method is more expensive than the artificial I/O spring formulation in computation. One reason for this is that the finite element with 12 nodal freedoms increases the computational expense of finite element analysis. The other reason is that all the freedoms of the output point o are considered by the proposed method, whereas the spring formulation only concerns the freedom u_x.

5.3.3 Displacement Redirector. This example illustrates the application in the case of single input and two outputs compliant mechanisms. The function of a displacement redirector is sketched in Fig. 17. The input port a is at the middle of the left side and causes two output displacement at ports b and c, respectively. The whole design domain is descretized using 100×100 finite elements for elastic analysis. The material usage is restricted to 20%. In this case, only the freedoms of the output ports b and c are considered, so the Jacobian matrix $\mathbf{J}$ of the displacement redirector is a 2×1 vector, whose desired form is shown in the following equation:

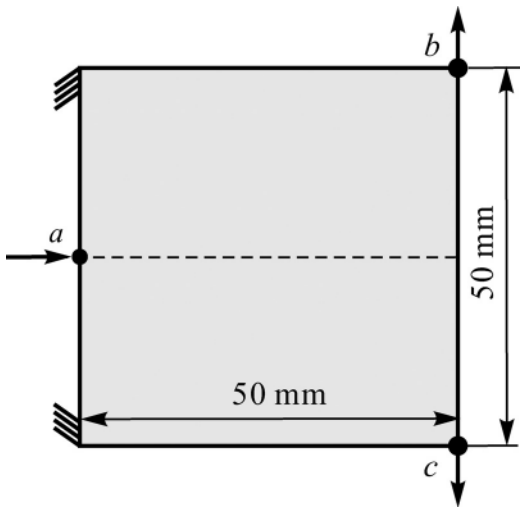

Fig. 17 Design domain for a displacement redirector

$$[u_b, u_c]^{\mathrm{T}} = [2, -2]^{\mathrm{T}} u_a \tag{41}$$

The corresponding topology optimization problem is solved by using the C-stiffness and stiffness formulations, respectively. The optimization process was run for 300 iterations. Figure 18(*a*) shows the resulting topology obtained by using the C-stiffness formulation and setting ω to 0.5. Its corresponding Jacobian matrix is $\mathbf{J} = [1.7, -1.7]^{\mathrm{T}}$. The C-stiffness at the input and output ports are 41.2, 5.9, and 5.9 N/mm, while the stiffness at input and output ports are 10.7, 2.3, and 2.3 N/mm, respectively. Figure 18(*b*) shows the resulting topology obtained by using the stiffness formulation and setting ω to 0.5. Its corresponding Jacobian matrix is $\mathbf{J} = [1.5, -1.5]^{\mathrm{T}}$. The C-stiffness at the input and output ports are 58.1, 4.1, and 4.1 N/mm, while the stiffness at input and output ports are 40.1, 3.3, and 3.3 N/mm, respectively. This case shows that the proposed method is applicable to the compliant mechanisms with multiple output ports, and both of the C-stiffness and stiffness formulations can obtain valid topologies.

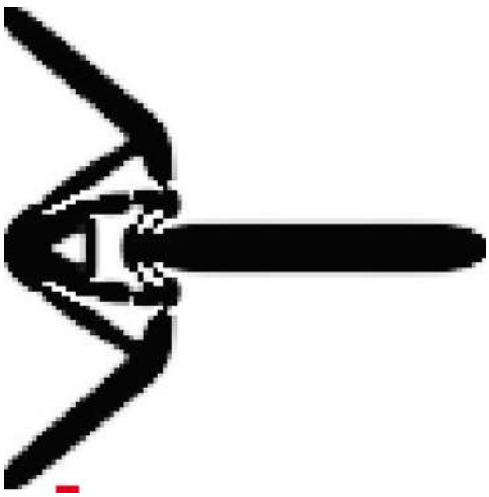

Fig. 16 Final topology of displacement amplifier designed by using the MSE/SE formulation

5.4 Analysis of Mesh Independency. This section is devoted to analyzing the mesh independency of the proposed method. The problem of 2DOF CPM, whose parameter settings except

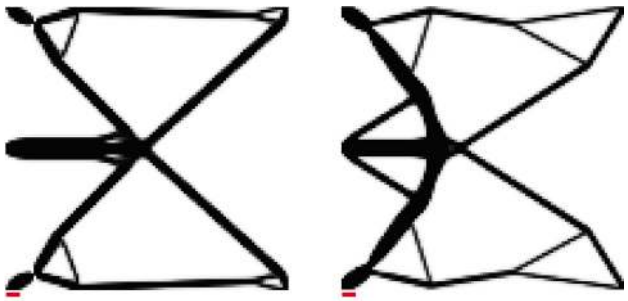

Fig. 18 Final topologies of displacement redirector solved by (*a*) the C-stiffness ($\omega = 0.5$) and (*b*) stiffness ($\omega = 0.5$) formulations

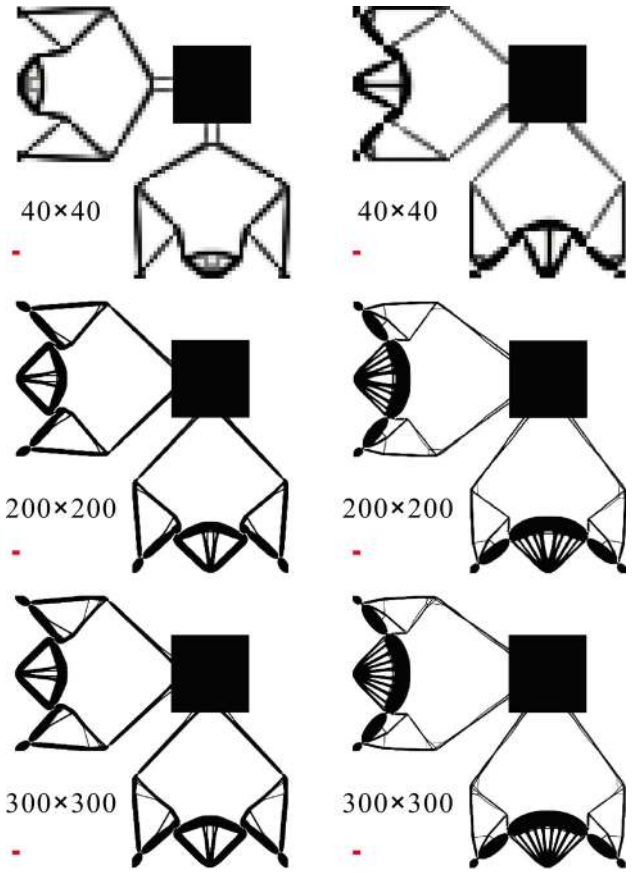

Fig. 19 Solutions obtained by using different element discretizations, and solved by the C-stiffness (left) and stiffness (right) formulations

discretization are the same as the case in Fig. 5, is used to illustrate the mesh independency. By using three different element discretizations of 40×40, 200×200 and 300×300, we obtain the corresponding results shown in Fig. 19. The three topologies on the left side of Fig. 19 are solved by the C-stiffness formulation, whereas the other side contains the results of the stiffness formulation. One can see that the results are almost stable under mesh refinement or mesh coarsening. In other words, the proposed method is mesh independent, which is ensured by the filtering technique of the 99 line MATLAB code.

6 Conclusions

This paper presents a new stiffness evaluation based on the definition of stiffness for the Jacobian-based topology optimization method. The proposed stiffness formulation is compared with the C-stiffness formulation by using two synthesis problems of CPMs and three traditional benchmark design problems. The results show that both of the two formulations can achieve valid topologies in most of design cases. In some cases like displacement amplifier, the C-stiffness formulation even the artificial I/O spring formulation cannot obtain valid result, while the stiffness formulation gives an improved stiffness evaluation. Besides, the Jacobian-based topology optimization method shows a general applicability in multi-DOF CPMs and benchmark design problems.

According to the results, the topologies produced by the proposed method are easy to exhibit hinges, especially when the kinematic requirement is much higher than stiffness requirement. Relatively speaking, the stiffness formulation has a better performance than the C-stiffness formulation in avoiding hinges, e.g., the two topologies in Fig. 18. The strategies for alleviating these hinges will be addressed in our future works.

Funding Data

- National Natural Science Foundation of China (Grant Nos. 51275174, 51605166, U1609206, and 51675189).
- Natural Science Foundation of Guangdong Province (Grant No. 2014A030313460).
- Fundamental Research Funds for the Central Universities.

References

[1] Howell, L. L., 2001, *Compliant Mechanisms*, Wiley, New York.
[2] Howell, L. L., and Midha, A., 1995, "Parametric Deflection Approximations for End-Loaded, Large-Deflection Beams in Compliant Mechanisms," ASME J. Mech. Des., **117**(1), pp. 156–165.
[3] Pucheta, M. A., and Cardona, A., 2010, "Design of Bistable Compliant Mechanisms Using Precision–Position and Rigid-Body Replacement Methods," Mech. Mach. Theory, **45**(2), pp. 304–326.
[4] Ananthasuresh, G. K., Kota, S., and Kikuchi, N., 1994, "Strategies for Systematic Synthesis of Compliant MEMS," ASME Paper No. DSC-55-2.
[5] Frecker, M. I., Ananthasuresh, G. K., Nishiwaki, S., Kikuchi, N., and Kota, S., 1997, "Topological Synthesis of Compliant Mechanisms Using Multi-Criteria Optimization," ASME J. Mech. Des., **119**(2), pp. 238–245.
[6] Nishiwaki, S., Frecker, M. I., Min, S., and Kikuchi, N., 1998, "Topology Optimization of Compliant Mechanisms Using the Homogenization Method," Int. J. Numer. Methods Eng., **42**(3), pp. 535–559.
[7] Sigmund, O., 1997, "On the Design of Compliant Mechanisms Using Topology Optimization," J. Struct. Mech., **25**(4), pp. 493–524.
[8] Howell, L. L., and Midha, A., 1996, "A Loop-Closure Theory for the Analysis and Synthesis of Compliant Mechanisms," ASME J. Mech. Des., **118**(1), pp. 121–125.
[9] Sigmund, O., 2001, "Design of Multiphysics Actuators Using Topology Optimization–Part I: One-Material Structures," Comput. Methods Appl. Mech. Eng., **190**(49), pp. 6577–6604.
[10] Sigmund, O., 2001, "Design of Multiphysics Actuators Using Topology Optimization–Part II: Two-Material Structures," Comput. Methods Appl. Mech. Eng., **190**(49), pp. 6605–6627.
[11] Saxena, A., 2005, "Topology Design of Large Displacement Compliant Mechanisms With Multiple Materials and Multiple Output Ports," Struct. Multidiscip. Optim., **30**(6), pp. 477–490.
[12] Lu, K.-J., and Kota, S., 2006, "Topology and Dimensional Synthesis of Compliant Mechanisms Using Discrete Optimization," ASME J. Mech. Des., **128**(5), pp. 1080–1091.
[13] Zhu, B., Zhang, X., and Wang, N., 2013, "Topology Optimization of Hinge-Free Compliant Mechanisms With Multiple Outputs Using Level Set Method," Struct. Multidiscip. Optim., **47**(5), pp. 659–672.
[14] Jang, G.-W., Lee, S., Kim, Y. Y., and Sheen, D., 2005, "Topology Optimization Using Non-Conforming Finite Elements: Three-Dimensional Case," Int. J. Numer. Methods Eng., **63**(6), pp. 859–875.
[15] Yamada, T., Izui, K., Nishiwaki, S., and Takezawa, A., 2010, "A Topology Optimization Method Based on the Level Set Method Incorporating a Fictitious Interface Energy," Comput. Methods Appl. Mech. Eng., **199**(45), pp. 2876–2891.
[16] Ansola, R., Veguería, E., Maturana, A., and Canales, J., 2010, "3D Compliant Mechanisms Synthesis by a Finite Element Addition Procedure," Finite Elem. Anal. Des., **46**(9), pp. 760–769.
[17] Jin, M., Zhang, X., Zhu, B., and Wang, N., 2013, "Spring-Joint Method for Topology Optimization of Planar Passive Compliant Mechanisms," Chin. J. Mech. Eng., **26**(6), pp. 1063–1072.
[18] Jin, M., Zhang, X., and Zhu, B., 2014, "A Numerical Method for Static Analysis of Pseudo-Rigid-Body Model of Compliant Mechanisms," Proc. Inst. Mech. Eng., Part C., **28**(17), pp. 3170–3177.
[19] Jin, M., Zhang, X., and Zhu, B., 2014, "Design of Compliant Mechanisms Using a Pseudo-Rigid-Body Model Based Topology Optimization Method," ASME Paper No. DETC2014-34325.
[20] Lum, G. Z., Teo, T. J., Yang, G., Yeo, S. H., and Sitti, M., 2013, "A Hybrid Topological and Structural Optimization Method to Design a 3-Dof Planar Motion Compliant Mechanism," IEEE/ASME International Conference on Advanced Intelligent Mechatronics (AIM), Wollongong, Australia, July 9–12, pp. 247–254.
[21] Lum, G. Z., Teo, T. J., Yang, G., Yeo, S. H., and Sitti, M., 2015, "Integrating Mechanism Synthesis and Topological Optimization Technique for Stiffness-Oriented Design of a Three Degrees-of-Freedom Flexure-Based Parallel Mechanism," Precis. Eng., **39**, pp. 125–133.
[22] Lum, G. Z., Teo, T. J., Yeo, S. H., Yang, G., and Sitti, M., 2015, "Structural Optimization for Flexure-Based Parallel Mechanisms-Towards Achieving Optimal Dynamic and Stiffness Properties," Precis. Eng., **42**, pp. 195–207.
[23] Jin, M., and Zhang, X., 2016, "A New Topology Optimization Method for Planar Compliant Parallel Mechanisms," Mech. Mach. Theory, **95**(1), pp. 42–58.
[24] Yong, Y. K., and Lu, T.-F., 2009, "Kinetostatic Modeling of 3-RRR Compliant Micro-Motion Stages With Flexure Hinges," Mech. Mach. Theory, **44**(6), pp. 1156–1175.
[25] Gao, Z., and Zhang, D., 2010, "Design, Analysis and Fabrication of a Multidimensional Acceleration Sensor Based on Fully Decoupled Compliant Parallel Mechanism," Sens. Actuators A, **163**(1), pp. 418–427.
[26] Chen, S., and Wang, M. Y., 2007, "Designing Distributed Compliant Mechanisms With Characteristic Stiffness," ASME Paper No. DETC2007-34437.

[27] Wang, M. Y., and Chen, S., 2009, "Compliant Mechanism Optimization: Analysis and Design With Intrinsic Characteristic Stiffness," Mech. Based Des. Struct. Mach., **37**(2), pp. 183–200.
[28] Wang, M. Y., 2009, "A Kinetoelastic Formulation of Compliant Mechanism Optimization," ASME J. Mech. Rob., **1**(2), p. 021011.
[29] Kim, C. J., Moon, Y.-M., and Kota, S., 2008, "A Building Block Approach to the Conceptual Synthesis of Compliant Mechanisms Utilizing Compliance and Stiffness Ellipsoids," ASME J. Mech. Des., **130**(2), pp. 284–284.
[30] Zhang, Y., Su, H.-J., and Liao, Q., 2014, "Mobility Criteria of Compliant Mechanisms Based on Decomposition of Compliance Matrices," Mech. Mach. Theory, **79**, pp. 80–93.
[31] Koseki, Y., Tanikawa, T., Koyachi, N., and Arai, T., 2000, "Kinematic Analysis of Translational 3-DOF Micro Parallel Mechanism Using Matrix Method," IEEE/RSJ International Conference on Intelligent Robots and Systems (IROS), Takamatsu, Japan, Oct. 31–Nov. 5, pp. 786–792.
[32] Bendsoe, M. P., and Sigmund, O., 2004, *Topology Optimization: Theory, Methods and Applications*, Springer, Berlin.
[33] Li, Y., and Xu, Q., 2009, "Design and Analysis of a Totally Decoupled Flexure-Based XY Parallel Micromanipulator," IEEE Trans. Rob., **25**(3), pp. 645–657.
[34] Sigmund, O., 2001, "A 99 Line Topology Optimization Code Written in Matlab," Struct. Multidiscip. Optim., **21**(2), pp. 120–127.
[35] Deepak, S. R., Dinesh, M., Sahu, D. K., and Ananthasuresh, G., 2009, "A Comparative Study of the Formulations and Benchmark Problems for the Topology Optimization of Compliant," ASME J. Mech. Rob., **1**(1), p. 011003.